PHYSICAL REVIEW A VOLUME 27, NUMBER 4 APRIL 1983

Wave propagation in media with focused gain

B. N. Perry, P. Rabinowitz, and M. Newstein*
Corporate Research-Science Laboratories, Exxon Research and Engineering Company, P. O. Box 45, Linden, New Jersey 07036
(Received 29 October 1982)

A solution of the scalar wave equation in a rotationally symmetric focused Gaussian amplifying medium is constructed from coupled Gaussian-Laguerre solutions of the free-space wave equation and is formally exact. The solution allows for the construction of the characteristic eigenmodes of the system and has direct application to Raman lasers, dye lasers, and the free-electron laser. The eigenvalues corresponding to the eigenmodes are directly related to mode growth rates and phase velocities. Numerical results for single- and multiple-pass growth are evaluated and exhibit an unpredicted gain enhancement that can be related to the phenomenon of "gain focusing" first described for uniform parabolic gain distributions. The solution for a focused parabolic gain distribution is also presented. Output intensity distributions are found for initial conditions corresponding to spontaneous emission and to a specified initial field. The same method of solution can be applied to a medium with a focused Gaussian refractive index.

I. INTRODUCTION

This paper addresses an important practical problem of coherent beam propagation in media in which a spatially nonuniform gain coefficient (gain function) is produced by a focused Gaussian beam.[1] This situation arises in laser amplifiers that are optically pumped, such as dye lasers and Raman lasers. It also arises in the free-electron laser, in which the gain is obtained from a focused electron beam. We show that for Raman lasers the output intensity distribution can be significantly different from that of the lowest-order free-space mode, regardless of the input field distribution. Also, the growth rate can be higher than that calculated on the basis of uncoupled mode growth. In our analysis, depletion of the gain function is not considered.

A similar problem of propagation in the presence of a transverse quadratic gain variation was previously analyzed by Kogelnik.[2] Cotter, Hanna, and Wyatt[3] applied Kogelnik's quadratic solution to the present case by replacing the Gaussian distribution with a parabolic one. To account for the focused gain function they used additional approximations. Other authors have also attempted to solve this problem.[4,5] They found the self-growth rates for some of the lower-order free-space modes, but did not consider the full problem including coupled mode effects which are necessary to properly describe propagation in all but the lowest gain limit. In this paper we show that if the gain function is proportional to the magnitude squared of a single rotationally symmetric Gaussian-Laguerre mode of free space and, in particular, to a focused Gaussian distribution, a formally exact solution of the scalar wave equation can be found.

II. FORMULATION

We begin with the scalar wave equation in the paraxial approximation. For free space

$$(\nabla^2+k^2)E=0; \tag{1}$$

where $k=2\pi\nu/c$ is the wave number of the propagating field. We seek solutions of the form $E(x,y,z)=\mathscr{E}(x,y,z)e^{i(2\pi\nu t-kz)}$ and neglect $\partial_z^2\mathscr{E}$ compared to $2k\,\partial_z\mathscr{E}$, to obtain the slowly varying envelope approximation to Eq. (1):

$$(\nabla_t^2-2ik\partial_z)\mathscr{E}=0\ , \tag{2}$$

where $\nabla_t^2=\partial_x^2+\partial_y^2$. In the presence of a prescribed gain function at each point in space, $G(x,y,z)$, we have

$$(\nabla_t^2-2ik\partial_z)\mathscr{E}=-ikG\mathscr{E}\ . \tag{3}$$

In this expression, the gain function is restricted to produce growth only over a distance of many wavelengths in order to preserve the validity of the slowly varying envelope approximation. When G has rotational symmetry, it is natural to use cylindrical coordinates. We now expand $\mathscr{E}$ in a complete set of

orthonormal Gaussian-Laguerre functions $U_p^l(r,\phi,z)$ which are solutions of Eq. (2) and are referred to as modes of free space[6];

$$\mathscr{E}(r,\phi,z)=\sum_{p,l} V_p^l(z)U_p^l(r,\phi,z;k,z_0)\ , \tag{4}$$

where the complex mode amplitudes $V_p^l(z)$ are functions only of z. The free-space modes U_p^l are functions of (r,ϕ,z) and depend on the parameter k [set equal to the wave number of Eq. (1)] and on z_0, the Rayleigh range, which is also half of what is called the confocal parameter and is left unspecified at this point. The explicit form of U_p^l is given in Appendix A. Substitution of Eq. (4) into Eq. (3), multiplication by $U_{p'}^{l'*}(r,\phi,z)$, and integration over the transverse coordinates, r and ϕ, gives the following set of ordinary linear coupled differential equations in z for the mode amplitudes:

$$\frac{dV_{p'}^{l'}(z)}{dz}=\sum_{p,l} G_{p'p}^{l'l}(z)V_p^l(z)\ , \tag{5}$$

where

$$G_{p'p}^{l'l}=\tfrac{1}{2}\int_0^{2\pi} d\phi \int_0^{\infty} r\,dr[U_{p'}^{l'*}G(r,z)U_p^l]\ . \tag{6}$$

To obtain Eq. (5) we have used the fact that the mode functions U_p^l are an orthogonal set of solutions of Eq. (2). Since we have taken the gain function $G(r,z)$ to be rotationally symmetric, the integration over ϕ in Eq. 6 results in nonzero terms only for $l=l'$. That is, only modes of the same rotational index l are coupled together by the gain. The mode coupling equation, Eq. (5), can thus be rewritten as a single sum over index p, namely,

$$\frac{d}{dz}V_{p'}^l(z)=\sum_p G_{p'p}^l(z)V_p^l(z)\ . \tag{7}$$

So far we have considered the gain to have an arbitrary rotationally symmetric shape; we now specialize to the case of a prescribed focused Gaussian gain, namely, one that is proportional to the magnitude squared of the lowest-order mode function U_0^0.[7] We then have

$$G(r,z)=g_0\,|\,U_0^0(r,z)\,|^2=\frac{2g_0e^{-2r^2/\omega_g^2}}{\pi\omega_g^2}\ . \tag{8}$$

The Gaussian spot size of the gain function, ω_g, is given by

$$\omega_g^2=\omega_g^2(o)[1+(z/z_0)^2]\ ,$$

where the parameters $\omega_g^2(o)=2z_0/k_g$, g_0, and k_g are specified by the gain. Since we are free to expand the field in terms of any complete set of free-space modes, we choose the value of z_0 in the field expansion of Eq. (4) as equal to the value established by the gain function of Eq. (8). We have chosen the two coordinate systems describing the gain function and the propagating field to have coincident origins (see Fig. 1). Evaluation of the coupling element $G_{p'p}^l(z)$ of Eq. (7) then gives (see Appendix A)

$$G_{p'p}^l=(\mu g_0/\pi\omega_g^2)\times\exp[-2i(p'-p)\tan^{-1}(z/z_0)]Q_{p'p}^l(\mu)\ . \tag{9}$$

The parameter μ, introduced here, is defined by

$$\mu=k/(k+k_g) \tag{10}$$

and measures the overlap of the gain and field intensity distributions. It is limited to the range $0<\mu<1$. The z-independent factor $Q_{p'p}^l(\mu)$ is a polynomial in μ.[8]

We now make a key substitution of variable for z in Eqs. (7) and (9), namely,

$$\theta=\tan^{-1}(z/z_0)$$

to obtain

$$\frac{dV_{p'}^l}{d\theta}=\sum_p M_{p'p}^l(\theta)V_p^l(\theta)\ , \tag{11}$$

where

$$M_{p'p}^l(\theta)=\mu G_p Q_{p'p}^l(\mu)e^{-2i(p'-p)\theta}\qquad(-\pi/2<\theta<\pi/2) \tag{12}$$

and where

$$G_p=g_0z_0/\pi\omega_g^2(o)\ .$$

We have introduced the quantity G_p to replace g_0 as a descriptive parameter, since G_p corresponds to the plane-wave field gain coefficient.[9] Because of the form of the gain function's dependence on z, the

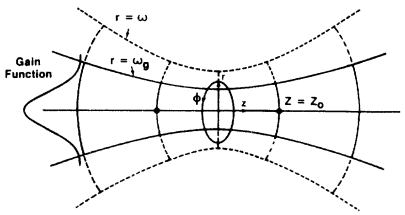

FIG. 1. Cylindrical coordinate system showing spot sizes of gain function and propagating field.

only θ dependence of Eq. (12) is contained in the exponential factors $e^{-2i(p'-p)\theta}$. We now cast Eq. (11) into explicit matrix form, with index p' labeling the rows of column vector $dV(\theta)/d\theta$ and of matrix $\underline{M}$ and index p labeling the columns of matrix $\underline{M}$ and the rows of vector $V(\theta)$. The rotational index l is a common superscript with each value labeling an independent set of equations. This is written as

$$\frac{dV^l}{d\theta}=\underline{M}^l(\theta)V^l(\theta) . \tag{13}$$

To simplify the notation, we drop the common index l.

III. SOLUTION

We now solve the system of Eq. (13) for a given l. From the θ dependence of Eq. (12), we can see that the matrix $\underline{M}$ is of the form

$$\underline{M}(\theta)=\underline{U}^{\dagger}(\theta)\underline{K}\,\underline{U}(\theta) ,$$

where $\underline{U}$ is a unitary matrix of the form $\underline{U}(\theta)=e^{i\underline{H}\theta}$, with $\underline{H}$ a constant diagonal (Hermitian) matrix whose elements are given by $H_{mn}=2m\delta_{mn}$.[10] Moreover, $\underline{K}$ is a constant, real symmetric matrix with elements

$$K^l_{p'p}=G_pQ^l_{p'p}(\mu) .$$

For convenience, we introduce the vector $Y(\theta)=\underline{U}(\theta)V(\theta)$. Solving for $V(\theta)$ and then taking the derivative with respect to θ, we obtain

$$V(\theta)=\underline{U}^{\dagger}(\theta)Y(\theta) ,$$

$$\frac{dV(\theta)}{d\theta}=\left[\frac{d}{d\theta}\underline{U}^{\dagger}\right]Y+\underline{U}^{\dagger}\frac{dY}{d\theta} , \tag{14}$$

$$\frac{dV(\theta)}{d\theta}=i\underline{H}\,\underline{U}^{\dagger}Y+\underline{U}^{\dagger}\frac{dY}{d\theta} .$$

Substituting Eq. (14) into Eq. (13) for $dV/d\theta$ we have, after some manipulation,

$$\frac{dY}{d\theta}=(\underline{K}+i\underline{H})Y(\theta) , \tag{15}$$

$\underline{K},\underline{H}$ independent of θ. The formal solution for Y is

$$Y(\theta)=[\exp(\underline{K}+i\underline{H})(\theta-\theta_0)]Y(\theta_0) , \tag{16}$$

and the solution for V is

$$V(\theta)=\underline{U}^{\dagger}(\theta)\exp[(\underline{K}+i\underline{H})(\theta-\theta_0)] \times\underline{U}(\theta_0)V(\theta_0) . \tag{17}$$

In Eq. (16) a power-series representation is always available for the exponential matrix operator since the exponential function is analytic everywhere. A more useful representation of Eq. (16) is in terms of the eigenvectors of the matrix $\underline{K}+i\underline{H}$. With an arbitrary real symmetric matrix $\underline{K}$, one may construct matrices $\underline{K}+i\underline{H}$ which cannot be diagonalized by a similarity transformation, or equivalently, whose eigenvectors do not span the entire space.[11] However, the physical situation under consideration here does not appear to admit such a possibility, and for all cases we have considered, an explicit solution for $V(\theta)$ is available through diagonalization, that is,

$$\underline{S}^{-1}(\underline{K}+i\underline{H})\underline{S}=\underline{D} , \tag{18}$$

where $\underline{D}$ is a constant diagonal matrix of the eigenvalues of $\underline{K}+i\underline{H}$, and $\underline{S}$ is a constant nonsingular matrix whose columns are the corresponding eigenvectors. The solution of Eq. (13) can then be expressed as

$$V(\theta)=\underline{A}(\mu,G_p;\theta,\theta_0)V(\theta_0) , \tag{19}$$

where

$$\underline{A}(\mu,G_p;\theta,\theta_0)=\underline{U}^{\dagger}(\theta)\underline{S}e^{\underline{D}(\theta-\theta_0)}\underline{S}^{-1}\underline{U}(\theta_0) .$$

The matrix diagonalization procedure, in addition to yielding the spatial evolution of an arbitrary input field, also gives the complete set of eigenmodes of the electromagnetic system with gain. These are found by choosing the vector V to be such that the corresponding vector Y is an eigenvector of the matrix $\underline{K}+i\underline{H}$. In contrast to the free-space modes, the eigenmodes of a system with gain are obtained from eigenvectors of a non-Hermitian operator and are not orthogonal. The amplitude of an eigenmode field $\mathscr{E}(r,\theta)$ reproduces itself at different values of the propagation variable θ in precisely the same sense as do the free-space modes. That is, it can be shown that the eigenmode field amplitudes at two different values of θ are identical complex functions of (r/ω) when the transverse coordinate is measured along surfaces whose curvature is equal to that of the free-space modes. The two fields then differ only by a normalization factor and the propagation factor $\exp[(\lambda+i)(\theta_2-\theta_1)]$, where λ is the corresponding complex eigenvalue. When the gain vanishes the eigenvalue λ equals $2pi$, and the free-space result is recovered.

Another related configuration of interest arises through periodic refocusing of the radiation field into regions with focused Gaussian gain.[12,13] We will now generalize the discussion to treat such multiple-pass cases. In Appendix B we show that this configuration leads to the same formal solution for the vector Y, Eq. (16), as for the single-pass case if the variable θ, which was defined in the range $-\pi/2<\theta<\pi/2$, is extended beyond $\pi/2$ without limit as the number of refocusings increases.[14] Thus, the eigenmodes and eigenvalues found for the

single-pass case continue to describe propagation in the multiple-pass case.

To this point, we have considered only a Gaussian gain distribution. To treat a system which includes a nonuniform refractive index with the same functional form as the gain function G, we note that we may redefine G in Eq. (3) to be complex. That is, we write

$$G'(r,z)=G(r,z)+2ikN(r,z) , \tag{20}$$

where N is real, but with the additional requirement that $|N| \ll 1$, in order to maintain the validity of the paraxial approximation. This effectively requires that the phase perturbation per unit wavelength produced by the variable refractive index be small compared with 2π. For the case of a focused Gaussian refractive index and no gain, the character of the solution changes since energy is conserved. The matrix $\underline{K}+i\underline{H}$ then becomes equal to i times a Hermitian matrix. Thus for a pure refractive index a unitary transformation can always be found to diagonalize $\underline{K}+i\underline{H}$ and solutions equivalent in form to Eq. (19) always exist.

IV. DISCUSSION OF THE RESULTS

We have found a solution for the mode coefficients $V(\theta)$ in Eq. (19);

$$V(\theta)=\underline{A}(\mu,G_p;\theta,\theta_0)V(\theta_0) ,$$

where $0<\mu<1$ and $0<G_p<\infty$. The solution depends on the wave-number ratio $\mu=k/(k+k_g)$, the plane-wave gain coefficient G_p, initial and final values of the propagation variable θ, and initial conditions $V(\theta_0)$. The formally exact solution corresponds to the inclusion of an infinite number of modes. However, we numerically solve Eq. (19) by truncation of the mode expansion to a finite number of modes of lowest order. In general, each truncation gives a different result. We have found, by examining the eigenvalues of the matrix $\underline{K}+i\underline{H}$ for 10, 20, 40, and 80 mode truncation, that truncation to 40 modes gives convergence of the eigenvalues if $\mu>0.05$ and the plane-wave gain coefficient G_p is less than 50, the regime for which we present results. We confirmed the operation of the numerical procedure used for diagonalization by evaluating the largest off-diagonal element in the matrix $\underline{D}$. This element was always $<10^{-12}$ of the largest diagonal element. Also, we will show that for initial conditions corresponding to equal energy in all free-space modes, or for that matter to all of the initial energy in the lowest mode, only the lowest 20 modes are sensibly populated after a quasi-steady-state mode distribution is established through coupled growth.

It is instructive to consider the solution when the field expansion is truncated to the single free-space mode of lowest order, U_0^0. Equation (11) becomes, with $Q_{00}^0(\mu)=1$,

$$\frac{dV_0^0(\theta)}{d\theta}=\mu G_p V_0^0(\theta) . \tag{21}$$

The lowest-order mode then grows at a rate given by μG_p, a result that had been obtained previously for stimulated Raman amplification by ignoring mode coupling.[12,5] The effect of including higher-order free-space modes is to allow for energy flow between free-space modes of a given rotational index l, as well as overall growth in the total field energy.

A. The eigenvalues and eigenmodes

Generalized field "growth rates" of the characteristic eigenmodes may be idenitified as the real parts of the eigenvalues of the matrix $\underline{K}+i\underline{H}$, while the imaginary parts of the eigenvalues give corrections to the phase velocities of the corresponding eigenmodes. Figure 2(a) shows a plot of the real

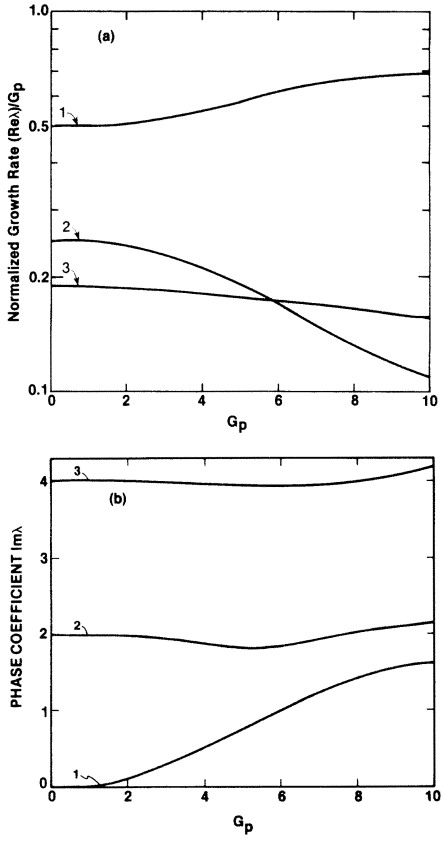

FIG. 2. (a) Normalized real parts of eigenvalues vs plane-wave gain coefficient G_p for $\mu=0.5$. (b) Corresponding imaginary parts of eigenvalues.

parts of the first three eigenvalues normalized to the plane-wave gain coefficient G_p, as functions of G_p, and Fig. 2(b) shows the corresponding imaginary parts of the eigenvalues. In Figs. 2(a) and 2(b) the value of the overlap parameter is $\mu=0.5$. One can see from Fig. 2(a) that the real parts of the eigenvalues appear as continuous functions of the plane-wave gain coefficient G_p if their numbering order is chosen at a particular value of G_p and analytically continued throughout the plot. We have chosen to number the eigenvalues in Fig. 2(a) at a value of G_p approaching zero. The ordering is done according to descending size of the real part of the eigenvalues, or equivalently according to increasing imaginary part. For vanishing gain this ordering procedure is identical to that usually adopted to order the free-space modes. In Fig. 2(a), the first eigenmode always has a dominant growth rate.

Figure 3(a) is a plot of the normalized real parts of the first nine eigenvalues which were similarly chosen at $G_p \to 0$ but for $\mu=0.05$. In contrast to the previous case of $\mu=0.5$, no single eigenmode is everywhere dominant. Instead, as the plane-wave gain is increased from zero, the real parts of the first, second, and successive eigenvalues are dominant in turn until at a value of $G_p=22$ the sixth eigenmode becomes dominant, and remains so as G_p is further increased. With inclusion of nine modes at $G_p \to 0$, the eigenmodes having the three highest growth rates have been retained for the values of $G_p \leq 30$ shown in Fig. 3(a). In Fig. 3(b), the imaginary parts of the eigenvalues of the first nine modes are shown as functions of G_p for $\mu=0.05$. For values of the plane-wave gain coefficient $G_p \geq 22$, large perturbations are introduced into the phase coefficients of the sixth and seventh modes, in the gain regime where the sixth eigenmode achieves final dominance of the growth rates. The eigenmodes having the largest growth rates will become exponentially dominant in size as the field propagation variable θ is increased [see Eq. (16)]. For the remainder of this paper we will therefore reorder the eigenvalues at fixed values of the parameters μ and G_p so that their real parts appear in descending size. The highest growth rate, which we will refer to as $G_{\max}$, then corresponds to the first eigenmode of the system. For values of μ, G_p, and $\theta-\theta_0$ such that the first eigenmode has dominant gain, the output fields can be described in terms of the first eigenmode, making the output radiation independent of the input spatial field distribution in that regime. The output fields can then be written as

$$|V_i(\theta)| \to |S_{i0}| e^{\mathrm{Re}D_{00}(\theta-\theta_0)} \left| \sum_j S_{0j}^{-1} V_j(\theta_0) e^{2i\theta_0} \right| . \tag{22}$$

In Fig. 4 we have plotted the dominant growth

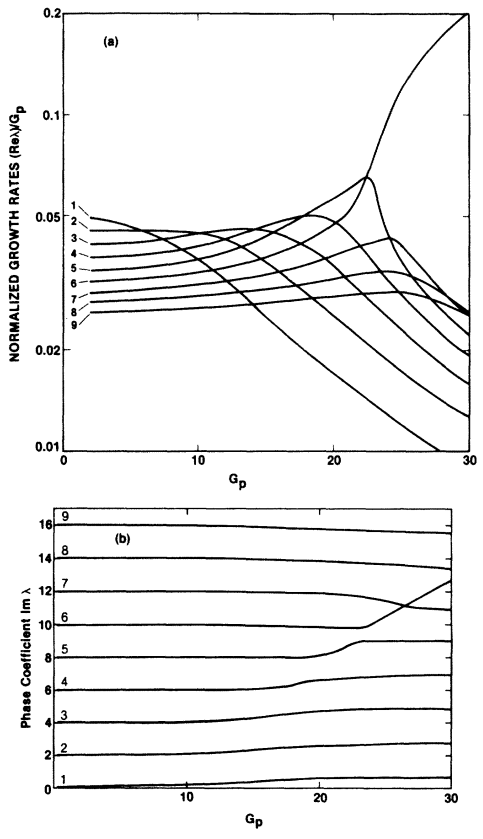

FIG. 3. (a) Normalized real parts of eigenvalues vs plane-wave gain coefficient G_p for $\mu=0.05$. (b) Corresponding imaginary parts of eigenvalues.

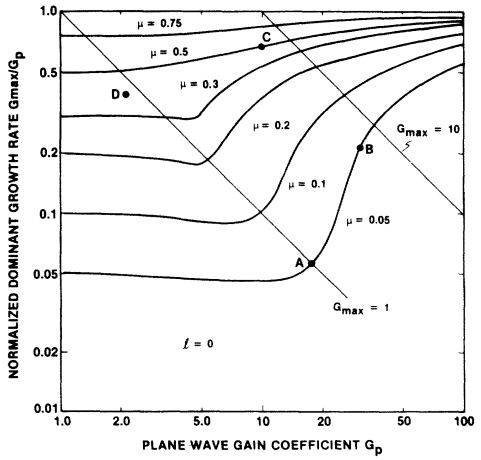

FIG. 4. Normalized dominant growth rates for rotationally symmetric eigenmodes.

rate, normalized to the plane-wave gain coefficient G_p, as a function of G_p, with μ as a parameter for $l=0$. For values of $\mu=0.3$, 0.2, 0.1, and 0.05, the plotted curves are, in fact, envelopes of families of curves of the type shown in Fig. 3(a), and are therefore not analytic. A similar plot for the group of modes of the next higher rotational order, namely, those with rotational index l equal to 1, is shown in Fig. 5.

We have evaluated and plotted in Figs. 6(a) and 6(b) and 7(a) and 7(b) the eigenmode fields for two specific cases. The figures show the magnitudes and phase distributions of the first three eigenmode fields ordered according to decreasing size of the real parts of their eigenvalues. They are shown as functions of the normalized radial coordinate r/ω for the parameter values $\mu=0.5$, $G_p=10$, and for $\mu=0.05$, $G_p=30$. In Figs. 6(a) and 7(a) each eigenmode field magnitude has been scaled so that its maximum value is unity for clarity of presentation. The quadratic phase factor $e^{-ikr^2/2R}$ common to all free-space modes has been suppressed in Figs. 6(b) and 7(b) so that the phase variation plotted against the radial coordinate represents the deviation from the free-space mode curvature. The corresponding eigenvalues can be found in Figs. 2 and 3 at the values of $G_p=10$ and 30, respectively.

Having obtained the eigenmodes, one also has the solution for the gain-filled resonator problem where the resonator mirrors match the phase curvature of the free-space modes. We note that when unmatched reflectors are used to construct a resonator, and a single eigenmode is dominant, the effective losses of the resonator can be large. With unmatched reflectors, upon reflection from a mirror, only a fraction of the field remains in the first eigenmode and continues to grow at a rapid rate. The solution for more general resonators that contain empty regions as well as regions of focused Gaussian gain may be found analogously by calculating the eigenmodes of the composite structure. This technique will be particularly useful in optimizing the output mode distribution from devices such as laser-pumped dye lasers and free-electron lasers.

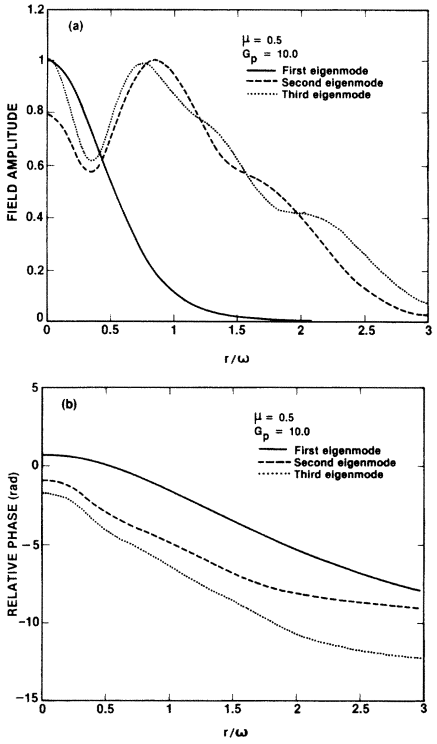

FIG. 6. (a) Magnitudes of eigenmode fields vs normalized radial coordinate. (b) Eigenmode phase deviations from free-space mode curvature vs normalized radial coordinate.

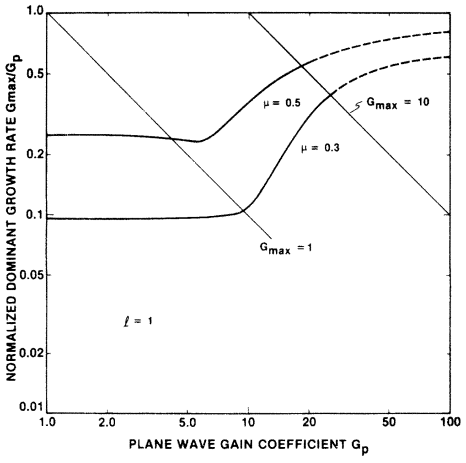

FIG. 5. Normalized dominant growth rates for higher rotational order ($l=1$) eigenmodes. Solid curves were obtained numerically and the dashed curves indicate qualitative behavior at higher gain.

B. Gain focusing

The rapid increase in the normalized growth rate of the sixth eigenmode of Fig. 3(a), or for that matter, the similar behavior of $G_{\max}$ as a function of G_p in Figs. 4 and 5 may at first sight appear surprising. Moreover, as the normalized growth rate $G_{\max}$ increases, the normalized growth rates of the other eigenmodes must decrease. The latter effect is a consequence of the invariance of the trace of the matrix $\underline{K}+i\underline{H}$ under the similarity transformation $\underline{S}$ used to accomplish diagonalization and is also ap-

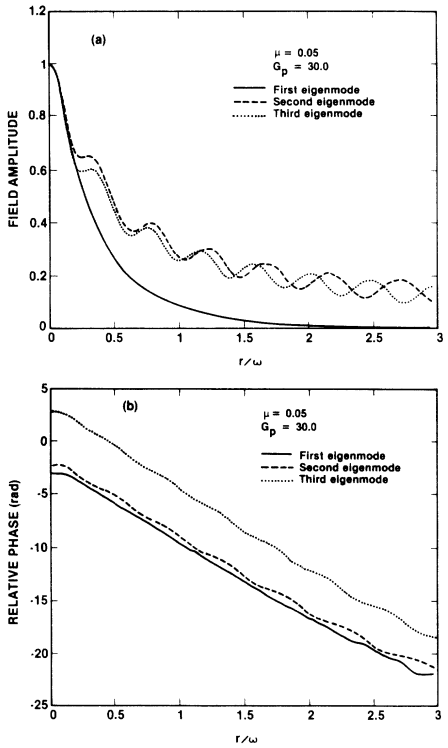

FIG. 7. (a) Magnitudes of eigenmode fields vs normalized radial coordinate. (b) Eigenmode phase deviations from free-space mode curvature vs normalized radial coordinate.

parent in Figs. 2(a) and 3(a). The rapid increase in $G_{\max}$ occurs when $G_{\max}\sim 1$, and is an indication of the onset of a regime where the gain dominates diffraction. The effect is more highly pronounced for small values of μ. In the limit of an infinitely large plane-wave gain coefficient, the eigenmode distribution approaches a delta function since the on-axis gain exponentially dominates. As the gain coefficient is increased towards that limit, the dominant eigenmode distribution narrows and becomes sensitive only to the spatial peak of the Gaussian gain distribution. As a consequence, the dominant growth rate approaches the plane-wave gain coefficient as indicated in Figs. 4 and 5. When the gain coefficient has become sufficiently large to confine the eigenmode field to an axial region narrower than the waist of the Gaussian gain function, the radial dependence of the gain function itself can be approximated by a parabolic distribution. In this approximation the results exhibit the phenomenon of gain focusing first described by Kogelnik[2] for a uniform parabolic distribution.

In the limit of high gain the dominant eigenmode field ψ for $l=0$ is given by a Gaussian distribution of the form

$$\psi(r,\theta)=(1/\omega_m)\times\exp[-r^2/\omega_m^2-i(kr^2/2R+Ar^2/\omega^2)]\ , \tag{23}$$

where $\omega_m^2=\omega_m^2(o)[1+(z/z_0)^2]$, A is a constant, and the parameters k, R, and ω are as defined in Eq. (A1) of Appendix A.

The solution can be verified by substituting the product of ψ and the complex propagation factor $\exp\lambda(\theta-\theta_0)$ into the wave equation, Eq. (3), with the Gaussian gain function $G(r,z)$ replaced by its expansion to second order in r, that is,

$$G(r,z)=(2g_0/\pi\omega_g^2)(1-2r^2/\omega_g^2)\ . \tag{24}$$

The substitution gives rise to the following relationships. The spot size ω_m is given by

$$\omega_m^4(o)=\frac{\omega^4(o)}{2G_p^2}\left[\frac{\mu}{1-\mu}\right]^2\times\left\{\left[1+4\left[\frac{1-\mu}{\mu}\right]^2G_p^2\right]^{1/2}-1\right\} \tag{25}$$

and the phase curvature coefficient A is

$$A=[\omega^4(o)/\omega_m^4(o)-1]^{1/2}\ . \tag{26}$$

The real part of the complex eigenvalue λ is given by

$$\mathrm{Re}\lambda=G_{\max}=G_p[1-\omega_m^2(o)/\omega_g^2(o)] \tag{27}$$

while the imaginary part of λ is given by

$$\mathrm{Im}\lambda=\omega^2(o)/\omega_m^2(o)\ . \tag{28}$$

Note that these relationships are valid only in the limit of high gain for the Gaussian gain function, but are exact for a focused parabolic gain distribution.[15]

C. Application to Raman amplifiers

In Raman amplifiers, gain is produced by focusing high intensity laser radiation into a Raman-active medium. Amplification can then occur for Raman-scattered radiation at wavelengths corresponding to excitation of a coherent polarization in the Raman medium. When the pump radiation is described by a $|U_0^0|^2$ intensity distribution, the preceding numerical results can be directly applied. We identify G_p as the plane-wave field gain coefficient per unit value of the propagation variable θ,

the parameter k as the wave number of the scattered radiation, and k_g as the wave number of the pump field. We note that for Stokes amplification the parameter μ defined in Eq. (10) takes on values $0<\mu<0.5$, while for amplification of anti-Stokes radiation its value is in the range $0.5<\mu<1$. For a single focused pass, the value of the propagation variable θ increases by a maximum value of π. As a result, the gain per pass of the first (dominant) eigenmode is $e^{\pi G_{\max}}$ and the corresponding power gain is $e^{2\pi G_{\max}}$. Figure 4 which gives normalized $G_{\max}$ as a function of μ and G_p is thus of paramount interest in understanding growth rates of Raman amplifiers. In superfluorescent amplifiers, e.g., single-pass Raman lasers, power gains of $\sim e^{30}$ typically occur in growth from spontaneous emission levels to detection thresholds. This corresponds to values of $G_{\max}\sim 5$. Lines of constant $G_{\max}$ have beeen plotted in Figs. 4 and 5 for values of $G_{\max}=1$ and 10, and roughly span the range over which single-pass amplifiers find application. As we have previously discussed, when the plane-wave gain is increased above $\mu G_p\sim 1$, a larger than linear increase in $G_{\max}$ occurs. This effect can lead to a dramatic reduction in threshold of Raman superfluorescent amplifiers. The effect is most significant for small values of μ, which are characteristic of Raman-Stokes lasers that employ visible pump lasers and amplify infrared radiation. For example, Fig. 4 indicates that for $\mu=0.05$ and $G_p=30$ the dominant growth rate is 3.5 times greater than the U_0^0 uncoupled result. At the other extreme, $\mu=0.5$, which is the upper limit of μ for Raman-Stokes lasers, the dominant growth rate is 30% larger than the uncoupled U_0^0 result for the value of $G_{\max}=5$. The latter is typical of a single-pass visible Raman laser. Therefore, an overestimate of the pump intensity required to reach threshold in stimulated Raman scattering can occur if the calculation is based on the uncoupled growth rate. However, for cases of small plane-wave gain the uncoupled growth rates provide an adequate description. Such cases are typical of multiple-pass Raman lasers where the radiation is periodically refocused to enhance the overall gain.

D. Propagation of higher-order rotational modes

So far in our discussion we have not included higher-order rotational modes in the field description. This does not affect the solutions for the most interesting amplifier case, that of a rotationally symmetric input field. Since modes of differing rotational order do not couple, the output cannot possess rotational character that is different from the input. When one considers an input generated by spontaneous emission, however, all modes have equal initial excitation and high-order rotational modes cannot simply be ignored. We have therefore obtained the dominant growth rates for the cases $l=1$, $\mu=0.5$ and $\mu=0.3$ which are plotted in Fig. 5. As the figure indicates, the gain is of the order of μ^2 times the plane-wave gain for low values of the plane-wave gain, and is always smaller than the corresponding growth rate for the symmetric modes. For example, in the case of $\mu=0.5$ and a growth to threshold of e^{30} for the $l=0$ dominant eigenmode, a growth of e^{15} occurs for the corresponding $l=1$ mode. This provides a ratio of at least five orders of magnitude between the output intensity of the rotationally symmetric modes and the next group of higher-order rotational modes. As a result, one can safely ignore growth in the higher-order rotational modes for superfluorescent Raman-Stokes lasers. Higher-order rotational modes could play a more significant role in anti-Stokes lasers for which $\mu\simeq 1$ and where nearly equal growth rates result.

E. Output intensity and decomposition into free-space modes

We have evaluated and plotted the output intensities and energy distribution in the free-space modes for several different values of the parameters μ and G_p that correspond to experimental configurations commonly used in stimulated Raman scattering. These plots correspond to the points A, B, C, and D in Fig. 4 which is the plot of the dominant growth rates for various values of μ. A description of the mathematical evaluation of the output intensities for both coherent and incoherent (spontaneous emission) input fields is found in Appendix C.

Figure 8 illustrates the output distribution of a single-pass amplifier for two different inputs; the

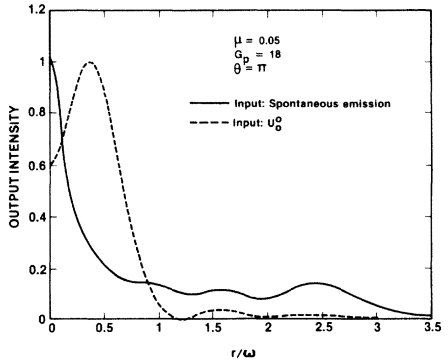

FIG. 8. Output intensity distributions for a single-pass amplifier.

output evolving from spontaneous emission is shown by the solid line and the output generated by a single mode U_0^0 input is shown by the dashed line. The values of μ and G_p correspond to point A in Fig. 4 and yield a value of $G_{\max} \cong 1$. For this case, we have shown that the first eigenmode is not dominant [see Fig. 3(a)]. As a result, the output intensity depends on the input field. Figures 9 and 10 show the output energy distribution in the free-space modes for the two inputs. It is interesting to note that although the intensity pattern evolving from the U_0^0 field input has a local minimum on axis, the output intensity contains more than two-thirds of its total power in the U_0^0 mode. In contrast, the amplified spontaneous emission intensity peaks on axis but has only about one percent of its total output in the U_0^0 mode. This case corresponds to a single-pass amplifier that has approximately 27 dB of gain, but realistically would not be used to amplify spontaneous emission.

In Figs. 11 and 12 the output intensity and mode distribution for point B in Fig. 4 are shown. This case corresponds to the same value of μ as in the previous figure but with a plane-wave gain that is about 60% greater than the gain in the previous case. With this relatively small increase in gain, the first eigenmode becomes dominant. As a result, the output is independent of the input, and input fields of either spontaneous emission or U_0^0 produce the same output field. For reference, the U_0^0 intensity is plotted as a dashed curve. Referring to Fig. 12, we note that about 20 free-space modes have significant power, with the peak of the distribution occurring at the seventh free-space mode.

Figures 13 and 14 correspond to the point C in Fig. 4 and show the intensity and the mode distribution that evolve from an arbitrary input field. This intensity pattern is in fact the square of the magnitude of the first eigenmode field distribution which was shown in Fig. 6. In contrast to previous cases, the spatial profile of the first eigenmode field magnitude is narrower than the gain function and may be fit with reasonable accuracy to a Gaussian distribution with a waist smaller than that of the U_0^0 mode. This phenomenon is related to the gain focusing effect that we have discussed. If the asymptotic result of Eq. (23) is applied to this case, one finds that the waists for the parabolic and Gaussian gain distribution differ by 18%; however, the growth rates ($G_{\max}$) differ by less than one percent. We have found that the two gain distributions produce nearly equal growth rates even for cases far from the asymptotic limit where the eigenmode field cannot be reasonably approximated by a Gaussian distribution.

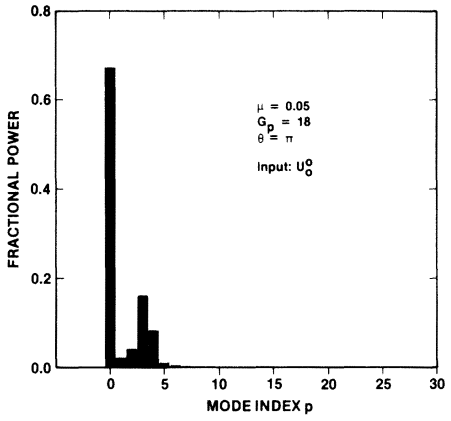

FIG. 10. Output power distribution in free-space modes for a single-pass amplifier.

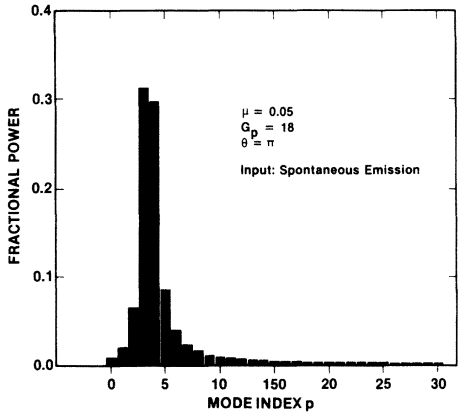

FIG. 9. Output power distribution in free-space modes for a single-pass amplifier.

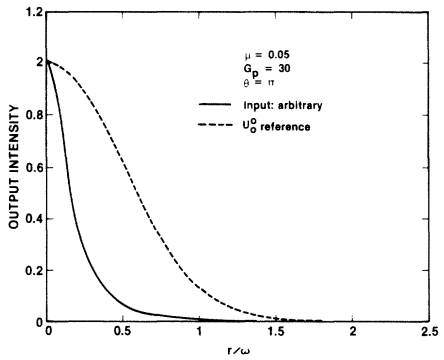

FIG. 11. Output intensity distribution for a single-pass amplifier and U_0^0 reference intensity.

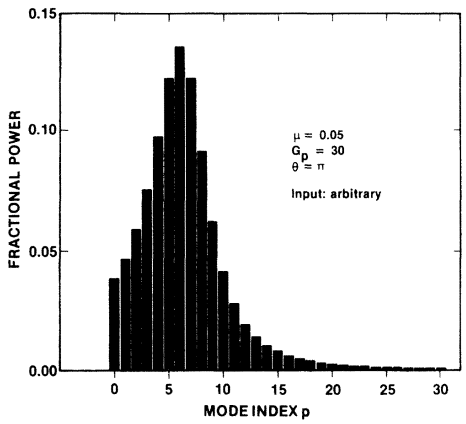

FIG. 12. Output power distribution in free-space modes for a single-pass amplifier.

Finally, Figs. 15 and 16 show the results for point D in Fig. 4. In these figures the values of μ, G, and θ correspond to the multiple-pass generation of 16-μm radiation from a 10.6-μm pump laser in H_2 by rotational Raman scattering.[12] Under these conditions, the deviation of the output from the U_0^0 mode is negligible and agrees closely with experiment.[16] These results also agree to within the numerical accuracy of a direct numerical integration of the wave equation which was used as an independent check of the validity of the formal solution.

V. CONCLUSION

While statements of the coupled mode field propagation problem in regions of focused Gaussian gain equivalent to Eq. (7) have been given previously,[17,18] and are implicit in the work of others,[19] to our knowledge this paper presents the first formally exact solution. The solution also yields the characteristic eigenmodes of the system with gain. Over most of the parameter space describing the spot size and strength of the focused gain, an eigenmode having a highly dominant growth rate can be found, and expressed as a linear combination of a relatively few free-space modes. Thus the expression is of practical utility for the rapid numerical solution of a large class of problems, among them the analysis of Raman lasers, dye lasers, and free-electron lasers, as we have shown. In this paper we have obtained results only for the case of a real gain function excluding the effects of dispersion. These results are representative of steady-state Raman or dye-laser amplification at the peak of an isolated gain resonance. However, to treat off-resonance propagation or more complicated dispersive media such as the free-electron laser, the full complex gain function must be employed. We are presently working to obtain solutions for those cases, as well as for that of pure refractive index media, and will present those results in a forthcoming paper.

APPENDIX A: EVALUATION OF COUPLING ELEMENTS

The orthonormal Gaussian-Laguerre solutions of Eq. (4) are written explicitly in cylindrical coordinates as[6]

$$U_p^l(r,\phi,z)=\frac{1}{\omega}\left[\frac{2p!}{\pi(l+p)!}\right]^{1/2}\left[\frac{\sqrt{2}r}{\omega}\right]^l L_p^l\left[\frac{2r^2}{\omega^2}\right]\exp\left\{\frac{-r^2}{\omega^2}-i\left[\pm l\phi+\frac{kr^2}{2R}-(2p+l+1)\tan^{-1}\left[\frac{z}{z_0}\right]\right]\right\}, \tag{A1}$$

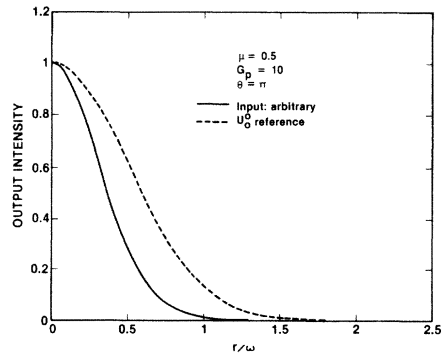

FIG. 13. Output intensity distribution for a single-pass amplifier and U_0^0 reference intensity.

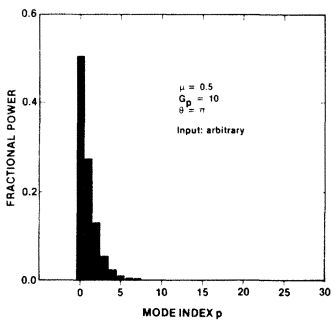

FIG. 14. Output power distribution in free-space modes for a single-pass amplifier.

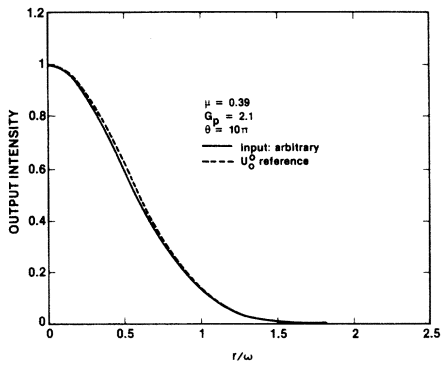

FIG. 15. Output intensity distribution for a multiple-pass amplifier (ten passes) and U_0^0 reference intensity.

where p and l are the radial and rotational indices, ω is conventionally called the spot size and is defined by $\omega^2=(2z_0/k)[1+(z/z_0)^2]$, k is the wave number, $2z_0$ is the confocal parameter, L_p^l are the associated Laguerre polynomials, and R is the phase front radius given by $R=z_0[(z/z_0)+(z_0/z)]$. Each value of the parameter z_0 produces a complete set of functions each of which is a solution of Eq. (2).

The gain function which is proportional to the squared magnitude of a single mode function $(U_p^{l*}U_p^l)$ can be written as

$$G_p^l=g_0\left[\frac{1}{\omega_g^2}\right]\left[\frac{2p!}{\pi(l+p)!}\right]\left[\frac{2r^2}{\omega_g^2}\right]^l \times\left[L_p^l\left[\frac{2r^2}{\omega_g^2}\right]\right]^2\exp\left[\frac{-2r^2}{\omega_g^2}\right], \tag{A2}$$

where g_0 is a constant and ω_g is the spot size of the gain function.

The gain coupling elements G_{hq}^s of Eq. (7) are given by

$$G_{hq}^s=\tfrac{1}{2}\int_0^{2\pi}d\phi\int_0^{\infty}r\,dr(U_h^{s*}G_p^lU_q^s)\,. \tag{A3}$$

The element G_{hq}^s is implicitly a function of the indices p and l which specify the gain function. Inserting explicit representations for U_h^{s*}, G_p^l, and U_q^s from Eqs. (A1) and (A2), we obtain

$$G_{hq}^s=B\int_0^{\infty}r\,dr\frac{\exp\{-2r^2[(1/\omega^2)+(1/\omega_g^2)]\}}{\omega^2\omega_g^2}\left[\frac{2r^2}{\omega_g^2}\right]^l\left[\frac{2r^2}{\omega^2}\right]^s\left[L_p^l\left[\frac{2r^2}{\omega_g^2}\right]\right]^2L_h^s\left[\frac{2r^2}{\omega^2}\right]L_q^s\left[\frac{2r^2}{\omega^2}\right], \tag{A4}$$

where

$$B=\frac{4g_0p!}{\pi(l+p)!}\left[\frac{h!q!}{(h+s)!(q+s)!}\right]^{1/2}\times\exp\left[2i(q-h)\tan^{-1}\left[\frac{z}{z_0}\right]\right].$$

We now let

$$x=2r^2[(1/\omega_g^2)+(1/\omega^2)]$$

and

$$\mu x=2r^2/\omega^2\,,$$

where

$$\mu=k/(k+k_g)\,. \tag{A5}$$

Equation (A4) can now be written as

$$G_{hq}^s=(B\mu/4\omega_g^2)\times\int_0^{\infty}dx\,e^{-x}(\mu x)^s[(1-\mu)x]^l\times[L_p^l((1-\mu)x)]^2L_h^s(\mu x)L_q^s(\mu x) \tag{A6}$$

or

$$G_{hq}^s=(B\mu/4\omega_g^2)I\,.$$

Since the integral I appearing in Eq. (A6) is a function only of the parameter μ and the indices l, p, s, and h, the value of G_{hq}^s can be written in a form similar to Eq. (9), with the z dependence made explicit:

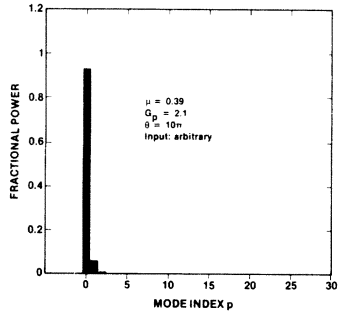

FIG. 16. Output power distribution in free-space modes for a multiple-pass amplifier.

$$G^s_{hq}=\frac{g_0\mu}{\pi\omega_g^2(o)}\frac{\exp[2i(q-h)\tan^{-1}(z/z_0)]}{1+(z/z_o)^2}\times Q^s_{hq}(\mu,l,p)\ , \tag{A7}$$

where

$$Q^s_{hq}(\mu,l,p)=\frac{p!}{(l+p)!}\left[\frac{h!q!}{(s+q)!(s+h)!}\right]^{1/2} I\ .$$

With the change of variables $\theta=\tan^{-1}(z/z_0)$, Eq. (A7) becomes

$$G^s_{hq}=\frac{g_0\mu}{\pi\omega_g^2(o)}\frac{\exp[2i(q-h)\theta]}{\sec^2\theta}Q^s_{hq}(\mu,l,p)\ , \tag{A8}$$

where the dependence of G^s_{hq} upon l and p explicitly appears in the polynomials Q^s_{hq}. This completes the evaluation of the coupling elements G^s_{hq}. Let us now recall that the indices h and q label the coupled free-space field modes of a given rotational index s, while the indices l and p denote the spatial character of the gain function. The continuous parameter μ is determined by the specified wave number k_g of the pump function and the field wave number through Eq. (A5). This result can be extended to treat a larger class of gain functions, each of which is expressed as a sum of magnitudes squared of single mode functions. The extension is straightforward since the dependence of the coupling elements G^s_{hq} upon θ is then identical to that of Eq. (A8).

We now evaluate the polynomial $Q^s_{hq}(\mu,l,p)$ for the case $l=p=0$ in order to derive a convenient closed-form expression. From Eqs. (A6) and (A7) we have

$$Q^s_{hq}(\mu,0,0)=\left[\frac{h!q!}{(h+s)!(q+s)!}\right]^{1/2}\times\int_0^\infty dx(\mu x)^s e^{-x}L^s_h(\mu x)L^s_q(\mu x)\ . \tag{A9}$$

We can expand $L^s_q(\mu x)$ in a power series[20] of $L^s_{q-m}(x)$, namely,

$$L^s_q(\mu x)=\sum_{m=0}^{q}\binom{q+s}{m}\mu^{q-m}(1-\mu)^m L^s_{q-m}(x)\ . \tag{A10}$$

Substituting into Eq. (A9) we get

$$Q^s_{hq}=\left[\frac{h!q!}{(h+s)!(q+s)!}\right]^{1/2}\int_0^\infty dx(\mu x)^s e^{-x}\sum_{m=0}^{q}\binom{q+s}{m}\mu^{q-m}(1-\mu)^m L^s_{q-m}(x)\times\sum_{n=0}^{h}\binom{h+s}{n}\mu^{h-n}(1-\mu)^n L^s_{h-n}(x)\ . \tag{A11}$$

We now use the orthogonality relations of the $L^s_{q-m}(x)$ to set $q-m=h-n$, and take $h\geq q$. Evaluation of the integral then gives

$$Q^s_{hq}(\mu)=\mu^s\left[\frac{h!q!}{(h+s)!(q+s)!}\right]^{1/2}\sum_{m=0}^{q}\binom{q+s}{m}\binom{h+s}{m+h-q}\frac{(q-m+s)!}{(q-m)!}\mu^{2(q-m)}(1-\mu)^{2m+h-q}\ ,\quad h\geq q\ . \tag{A12}$$

The results given in the text of this paper were obtained through explicit numerical evaluation of polynomials of the form Eq. (A12).

APPENDIX B: EXTENSION TO MULTIPLE-PASS AMPLIFICATION

In this appendix, we find the amplified field produced by periodic refocusing of radiation into focused Gaussian gain regions. We consider only cases symmetrical in z, mode-matched,[6] and with rotationally symmetric fields, although the most general case can also be treated in a similar fashion. We assume that the gain function is itself produced by a copropagating field (e.g., Raman pump) which is transformed by the optical system in the same manner as the propagating field.

Consider the system of Fig. 17. A field is introduced at $\theta=-\theta_1$ and propagated to $\theta=\theta_1$ through a Gaussian gain medium in region 1 of the figure. The field is then passed through a positive lens, which changes the sign of its phase front curvature.

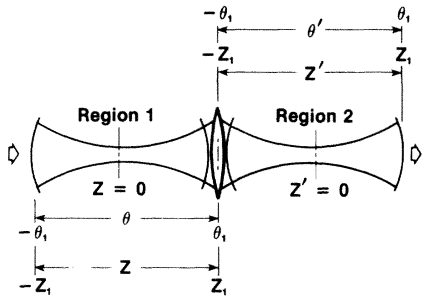

FIG. 17. Configuration and coordinate system for multiple-pass amplifier.

The field is then propagated through region 2, which has the same gain distribution as region 1. The propagation distance in region 2 is measured by coordinate z' (or θ'), and propagation is from $\theta'=-\theta_1$ to $\theta'=\theta_1$.

The field at $\theta=\theta_1$ is expressed in the unprimed coordinate system as

$$\mathscr{E}(r,z_1)=\sum_p V_p(\theta_1)e^{-ik(r^2/2R_1)}e^{i(2p+1)\theta_1}f_p(z_1,r)\ ,$$

where R_1 is evaluated at $z=z_1$, and where the function f_p is given by

$$f_p(z,r)=(2/\pi)^{1/2}(1/\omega)e^{-r^2/\omega^2}L_p^0(2r^2/\omega^2)\ .$$

The function f_p depends on z implicitly through $\omega(z)$, and is an even function of z. We recall that the mode coefficients $V_p(\theta=\theta_1)$ at the output of region 1 are related to the input mode coefficients $V_p(\theta=-\theta_1)$ through the fundamental solution in Eq. (19). At a location just after the positive lens we have

$$\mathscr{E}(r,z_1)=\sum_p V_p(\theta_1)e^{ikr^2/2R_1}e^{i(2p+1)\theta_1}f_p(z_1,r)\ ,$$

which is a function only of r. We now take this field as the imput to region 2, and identify the input mode coefficients for this region. We use the orthogonality relations of the functions f_p to obtain

$$V_p'(\theta'=-\theta_1)=e^{i2(2p+1)\theta_1}V_p(\theta_1)\ .$$

In our matrix notation this reads

$$V'(-\theta_1)=e^{2i\theta_1}\underline{U}^2(\theta_1)V(\theta_1)\ .$$

Applying Eq. (19) twice to accomplish the field propagation in both regions, we obtain

$$V'(\theta')=\underline{U}^\dagger(\theta')\underline{S}e^{\underline{D}(\theta'+\theta_1)}\underline{S}^{-1}e^{2i\theta_1}\underline{U}(-\theta_1)\times\underline{U}^2(\theta_1)\underline{U}^\dagger(\theta_1)\underline{S}e^{2\underline{D}\theta_1}\underline{S}^{-1}\underline{U}(-\theta_1)\times V(\theta=-\theta_1)\ .$$

Since $\underline{U}(-\theta_1)=\underline{U}^\dagger(\theta_1)$ and $\underline{U}$ is unitary,

$$\underline{S}^{-1}\underline{U}(-\theta_1)\underline{U}^2(\theta_1)\underline{U}^\dagger(\theta_1)\underline{S}=\underline{I}$$

where $\underline{I}$ is the identity matrix, and

$$V'(\theta')=\underline{U}^\dagger(\theta')\underline{S}e^{\underline{D}(\theta'+3\theta_1)}\underline{S}^{-1}\underline{U}(\theta_1)\times V(\theta=-\theta_1)e^{2i\theta_1}\ .$$

This equation is precisely of the form for a single focused pass, where the argument of the exponential operator $e^{\underline{D}\theta}$ is now increased by $2\theta_1\underline{D}$. The generalization to n completed passes is then

$$V'(\theta')=\underline{U}^\dagger(\theta')\underline{S}e^{\underline{D}[\theta'+(2n+1)\theta_1]}\underline{S}^{-1}\underline{U}(\theta_1)\times V(\theta=-\theta_1)e^{2ni\theta_1}\ .$$

Thus the eigenmodes and eigenvalues found for the single-pass case continue to describe propagation in the multiple-pass case.

For the case in which the gain function is not matched to the multiple-pass structure, the problem can be solved in a piecemeal manner. The propagating field is found after the first pass as previously through Eq. (19). The Gaussian beam relationships[6] are then used to calculate the transformed field parameters after transmission through the lens, in particular, the new values of the confocal parameter, the propagation variable θ, and the radius of curvature. The process is then repeated with the propagating field always expanded in a set of modes having the confocal parameter of the gain function.

APPENDIX C: EVALUATION OF FIELDS AND INTENSITIES

For convenience, we now reexpress the scalar electric field of Eq. (4) in equivalent matrix form as

$$\mathscr{E}(r,\theta)=W^T(r,\theta)V(\theta)\ , \tag{C1}$$

where W^T is a row vector of mode functions of the form $W^T=[U_0^l,U_1^l,\ldots,U_p^l]$ and $V(\theta)$ is a column vector with elements $V_p^l(\theta)$. The intensity at each point is then obtained using Eq. (19), and is given by

$$I(r,\theta)=\mathscr{E}(r,\theta)\mathscr{E}^*(r,\theta) \tag{C2}$$

or,

$$I(r,\theta)=W^T(r,\theta)A(\theta,\theta_0)V(\theta_0)V^\dagger(\theta_0)\times\underline{A}^\dagger(\theta,\theta_0)W^*(r,\theta)\ ,$$

where, from Eq. (19), $V(\theta)=\underline{A}(\theta,\theta_0)V(\theta_0)$. Although one can solve for the fields and intensities which evolve from any initial conditions, we will restrict ourselves to two cases, first to amplification of the lowest-order mode U_0^0, and second to amplification of spontaneous emission.

For the first case we can write the initial condition for the mode amplitudes as $V_i(\theta_0)=\delta_{i0}$. The output mode coefficients $V(\theta,\theta_0)$ are then given by the first column of the matrix $\underline{A}(\theta,\theta_0)$. Both the fields and the intensities can be obtained directly from Eqs. (C1) and (C2), respectively.

For the second case, that of amplification of spontaneous emission we find the total output intensity in each mode $|V_p(\theta)|^2$ in terms of the initial conditions, and then average over an ensemble with initial condition given by equal excitation in each mode, and no correlation between field amplitudes of the modes. In matrix notation, we use Eq. (19) to write

$$\langle V(\theta)V^{\dagger}(\theta)\rangle=\langle \underline{A}(\theta,\theta_0)V(\theta_0)V^{\dagger}(\theta_0)\underline{A}^{\dagger}(\theta,\theta_0)\rangle ,$$

where the brackets denote an ensemble average. Since the propagation matrix $\underline{A}(\theta,\theta_0)$ is independent of the ensemble member, and since

$$\langle V(\theta_0)V^{\dagger}(\theta_0)\rangle_{ij}=\delta_{ij}$$

describes the initial ensemble, we obtain

$$\langle V(\theta)V^{\dagger}(\theta)\rangle=\underline{A}(\theta,\theta_0)\underline{A}^{\dagger}(\theta,\theta_0) ,$$

whose diagonal elements are the mode energies. Similarly, the ensemble averaged intensity at each spatial point is obtained from Eq. (C2) to give

$$\langle I(r,\theta)\rangle=W^{T}(r,\theta)\underline{A}(\theta,\theta_0)\underline{A}^{\dagger}(\theta,\theta_0)W^{*}(r,\theta) .$$

---

*Permanent address: Polytechnic Institute of New York, Long Island Center, Farmingdale, New York 11735.

[1]B. N. Perry, P. Rabinowitz, and M. Newstein, Phys. Rev. Lett. 49, 1721 (1982).

[2]H. Kogelnik, Appl. Opt. 4, 1562 (1965).

[3]D. Cotter, D. C. Hanna, and R. Wyatt, Appl. Phys. 8, 333 (1975).

[4]W. R. Trutna, Jr. and R. L. Byer, Appl. Opt. 19, 301 (1980).

[5]R. T. V. Kung, IEEE J. Quantum Electron. QE-18, 1323 (1982).

[6]H. Kogelnik and T. Li, Appl. Opt. 5, 1550 (1966).

[7]More generally, the same procedure followed here applies if the gain function is the magnitude squared of any single mode function U_p^l, or a sum of the squares of such mode functions (see Appendix A).

[8]It can be shown that the polynomial $Q_{p'p}^{l}(\mu)$ can be simply related to a Jacobi polynomial of argument $(1-2\mu+2\mu^2)/(1-2\mu)$.

[9]The plane-wave field gain coefficient is usually defined for Raman lasers as the exponential growth rate that would apply if the peak gain coefficient were uniform in the transverse dimension as would occur in the limit $k_g\rightarrow 0$ or $\mu\rightarrow 1$.

[10]Because the mode indices begin at zero, we have chosen the row and column indices of our matrices to begin at zero.

[11]See, e.g., L. Mirsky, *An Introduction to Linear Algebra* (Oxford University Press, London, 1963), p. 294.

[12]P. Rabinowitz, A. Stein, R. Brickman, and A. Kaldor, Opt. Lett. 3, 147 (1978).

[13]R. L. Byer and W. R. Trutna, Jr., Opt. Lett. 3, 144 (1978).

[14]In the multiple-pass case, however, the value of θ which relates Y to V in Eq. (14), continues to have the restricted range $-\pi/2<\theta<\pi/2$.

[15]L. W. Casperson, Appl. Opt. 12, 2434 (1973).

[16]P. Rabinowitz, A. Stein, R. Brickman, and A. Kaldor, Appl. Phys. Lett. 35, 739 (1979).

[17]R. Asby, Phys. Rev. 187, 1062 (1969).

[18]W. R. Trutna, Jr., Edward L. Ginzton Laboratory Report No. 2977, Stanford University (unpublished).

[19]G. D. Boyd, W. D. Johnston, Jr., and I. P. Kaminow, IEEE J. Quantum Electron. QE-5, 203 (1969).

[20]*Handbook of Mathematical Functions,* edited by M. Abramowitz and I. A. Stegun (U.S. GPO, Washington D.C., 1966), p. 785.